Supplementary Information

A Parts-per-Million Scale Electrolyte Additive for Durable Aqueous Zinc Batteries

Shixun Wang,[1#] Shengnan Wang,[1#] Zhiquan Wei,[1] Yiqiao Wang,[1] Dechao Zhang,[2] Ze Chen,[1] Chunyi Zhi[1, 2*]

1 Department of Materials Science and Engineering, City University of Hong Kong, 83 Tat Chee Avenue, Hong Kong S.A.R., 999077, P. R. China

2 Hong Kong Center for Cerebro-Cardiovascular Health Engineering (COCHE), Shatin, NT, Hong Kong S.A.R., 999077, P. R. China

[*] Corresponding authors: cy.zhi@cityu.edu.hk

[#] The two authors contributed equally to this work.

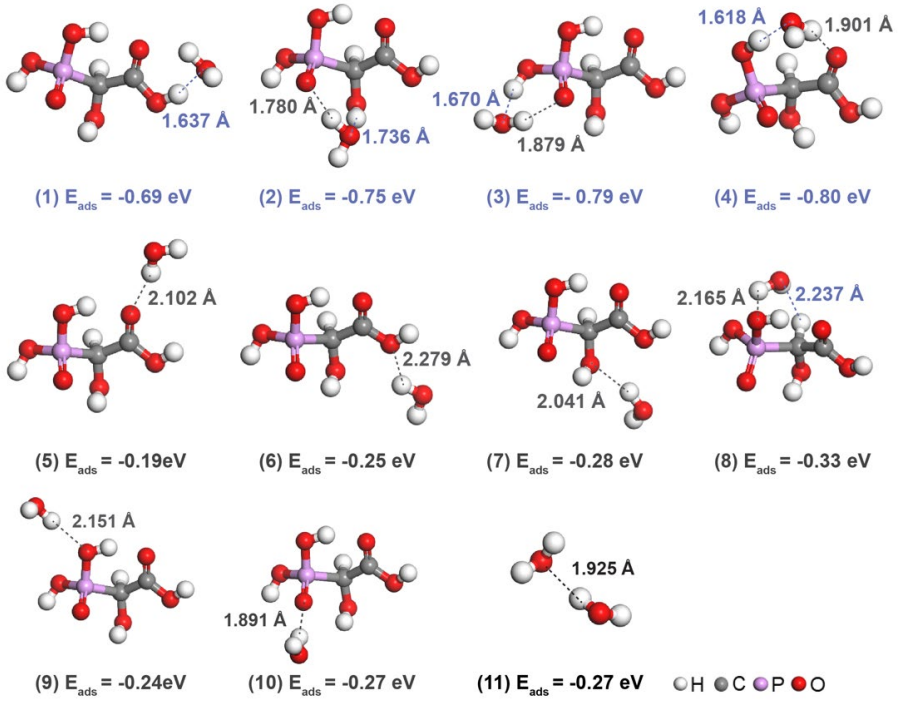

Supplementary Fig. 1 | DFT calculation of molecular interaction energy. 1-10 The intramolecular coordination between PPGA and H_2O and the corresponding bond energy; **11** the intermolecular coordination of H_2O.

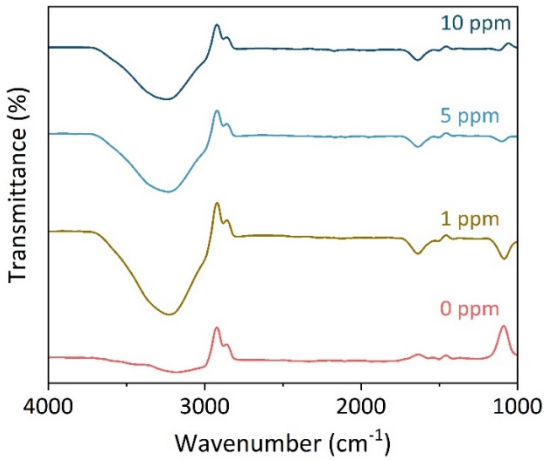

Supplementary Fig. 2 | FTIR result. FTIR spectra of BZS with a varying amount of PPGA (0, 1, 5, or 10 ppm).

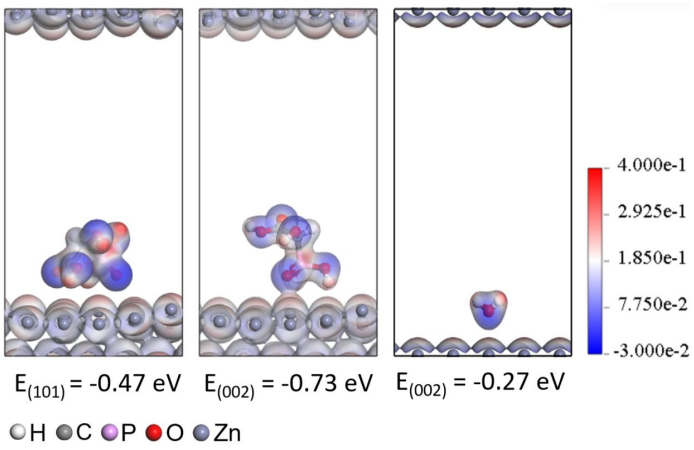

Supplementary Fig. 3 | Molecular adsorption on the zinc surface. The adsorption of PPGA on the (101) and (002) lattice plane of zinc (left), and the interaction between water and zinc metal (right), with electrostatic potential mapped on the surface of the electron density.

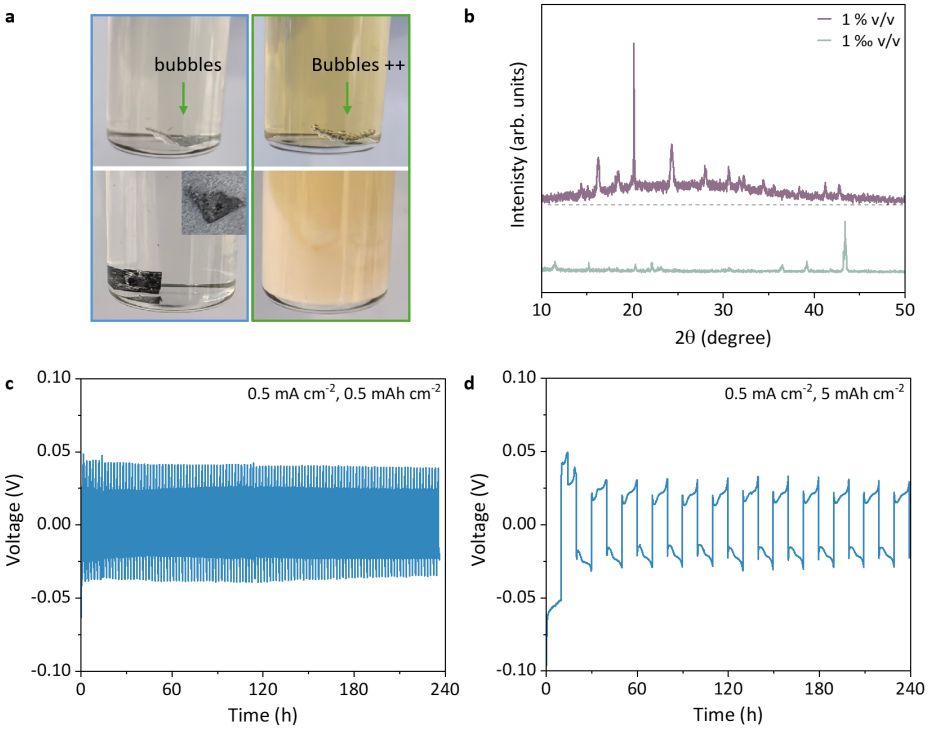

Supplementary Fig. 4 | Impact of the PPGA concentration on zinc metal. Photograph showing the immersion of zinc metal into aqueous **a** 0.1 % v/v (blue wireframe) and 1 % v/v (green wireframe) PPGA solutions and stored for 8 days; **b** XRD patterns of the zinc metal in **a**; Zn|PZS|Zn symmetric cells cycled at **c** 0.5 mA cm^{-2}, 0.5 mAh cm^{-2} and **d** 0.5 mA cm^{-2}, 5 mAh cm^{-2}.

Supplementary Note 1. The immersion treatment revealed ongoing corrosion of the zinc metal in a diluted aqueous PPGA solution. The 0.1% v/v PPGA solution partly dissolved the zinc metal and rendered it brittle after 8 days, as illustrated in the inset of Supplementary Fig. 4c. Remarkably, the zinc metal transformed into intricate white powders in the 1% v/v PPGA solution, unveiling the contrasting effect of concentrated PPGA on zinc. Subsequent cycling of Zn||Zn symmetric cells with 5 and 30 ppm PPGA indicated that a higher additive concentration may negatively impact battery performance. It could be attributed to the diminished crystal size of Zn post-PPGA treatment, as shown in Fig. 2b, c and would become more crucial during the stripping/plating process, necessitating further comprehensive studies within the research community.

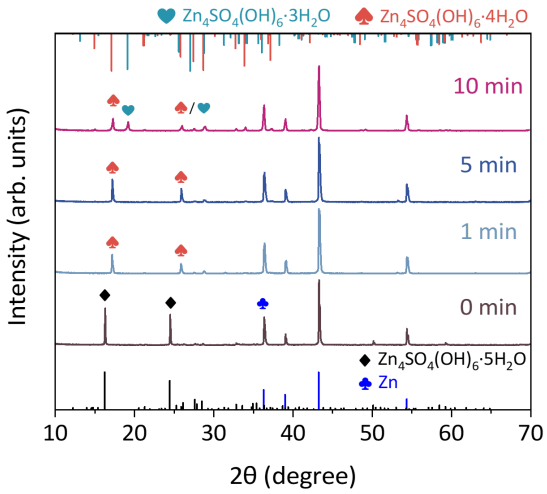

Supplementary Fig. 5 | XRD result. A wider field of view of the XRD pattern shown in Fig. 2b.

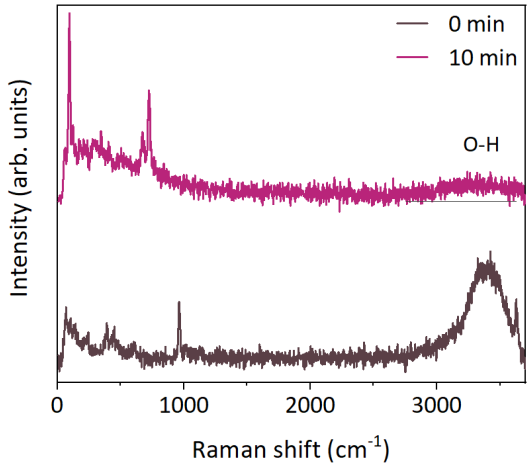

Supplementary Fig. 6 | Raman result. The Raman spectra of the "0 min" and "10 min" sample demonstrated in Fig. 2.

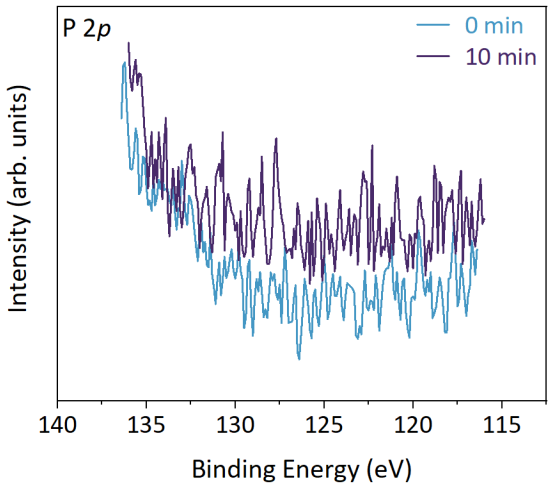

Supplementary Fig. 7 | High-resolution XPS result. The P 2*p* core level spectra of the zinc anode with and without 10 min of the proposed PPGA treatment in Fig. 2a.

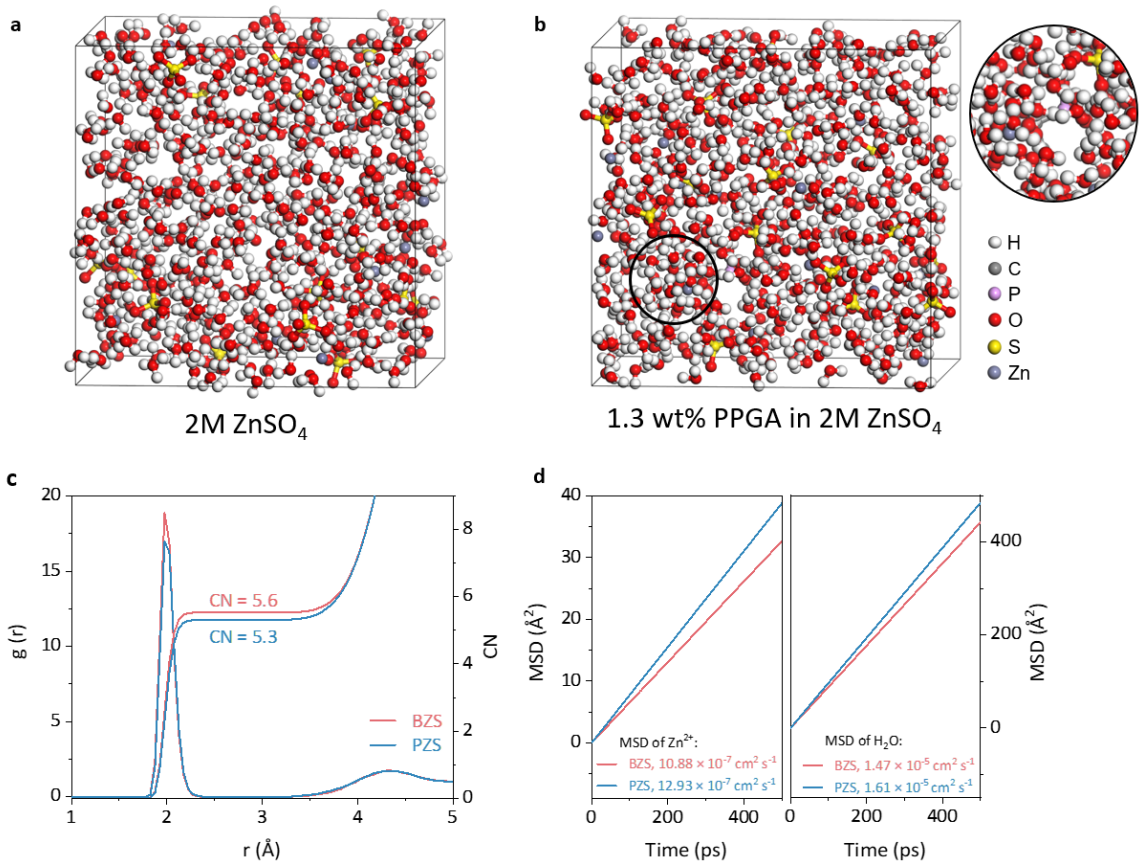

Supplementary Fig. 8 | MD simulation. 3D snapshot of **a** 2M $ZnSO_4$ and **b** 1.3 wt% PPGA in 2 M $ZnSO_4$ from MD simulation and partial enlarged snapshot representing the electrolyte structure (atoms in red, grey, white, pink and yellow denote oxygen, zinc, hydrogen, phosphorus and sulfur, respectively); **c** RDFs for Zn^{2+}-O (H_2O) and **d** MSD of Zn^{2+} and H_2O in the studied electrolytes.

Supplementary Note 2. The radial distribution function (RDF) study of Zn^{2+}-O interaction in Supplementary Fig. 8c suggested that the coordination number (CN) of Zn^{2+} reduced from 5.6 for BZS to 5.3 for the electrolyte contained PPGA, which pointed out a reducing number of coordinated waters in the first solvent sheath of Zn^{2+} in the latter case, favoring the desolvation process of $Zn(H_2O)_{5.6}^{2+}$ specifically at zinc surface as the accumulation of adsorbed PPGA. MD simulation results in Supplementary Fig. 8d showed that the mean squared displacement (MSD) of both Zn^{2+} and H_2O

slightly reduced as the inclusion of PPGA, corresponding to an optimized mobility Zn^{2+} and H_2O, which could help achieve smooth zinc flux and uniform deposition.

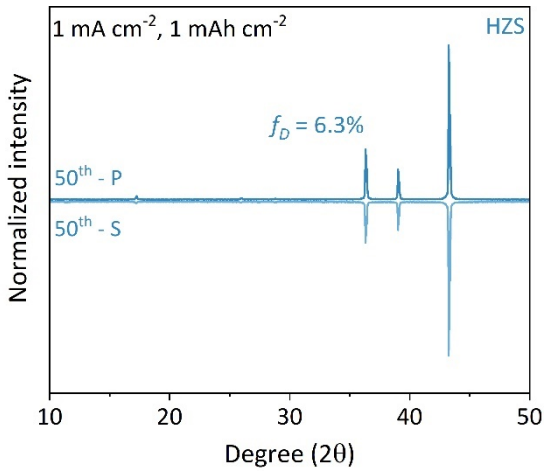

Supplementary Fig. 9 | XRD result of cycled zinc electrodes. XRD pattern of stripped/plated zinc electrodes in the Zn|PZS|Zn cell. We note that the electrodes were cycled at 25 °C.

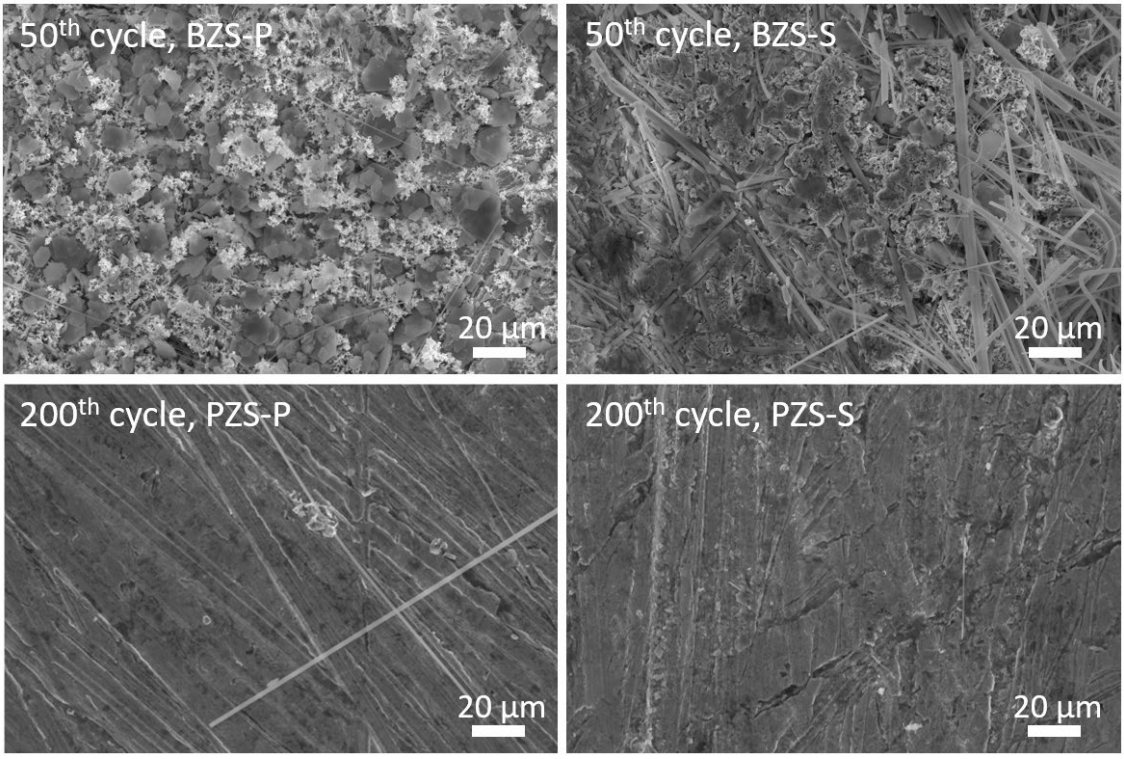

Supplementary Fig. 10 | Surface morphology of cycled zinc electrodes. SEM images of cycled Zn|BZS|Zn and Zn|PZS|Zn. "-P" and "-S" denote that the last cycle was plating and stripping of zinc, respectively. We note that the electrodes were cycled at 1 mA cm^{-2}, 1mAh cm^{-2} at around 25 ^{o}C.

Supplementary Note 3. The widespread dispersion of glass fibers in "BZS-S" can be attributed to the existence of Zn dendrites and the heterogeneous crystallization of Zn that extended to the separator, leading to undesired Zn stripping/plating.

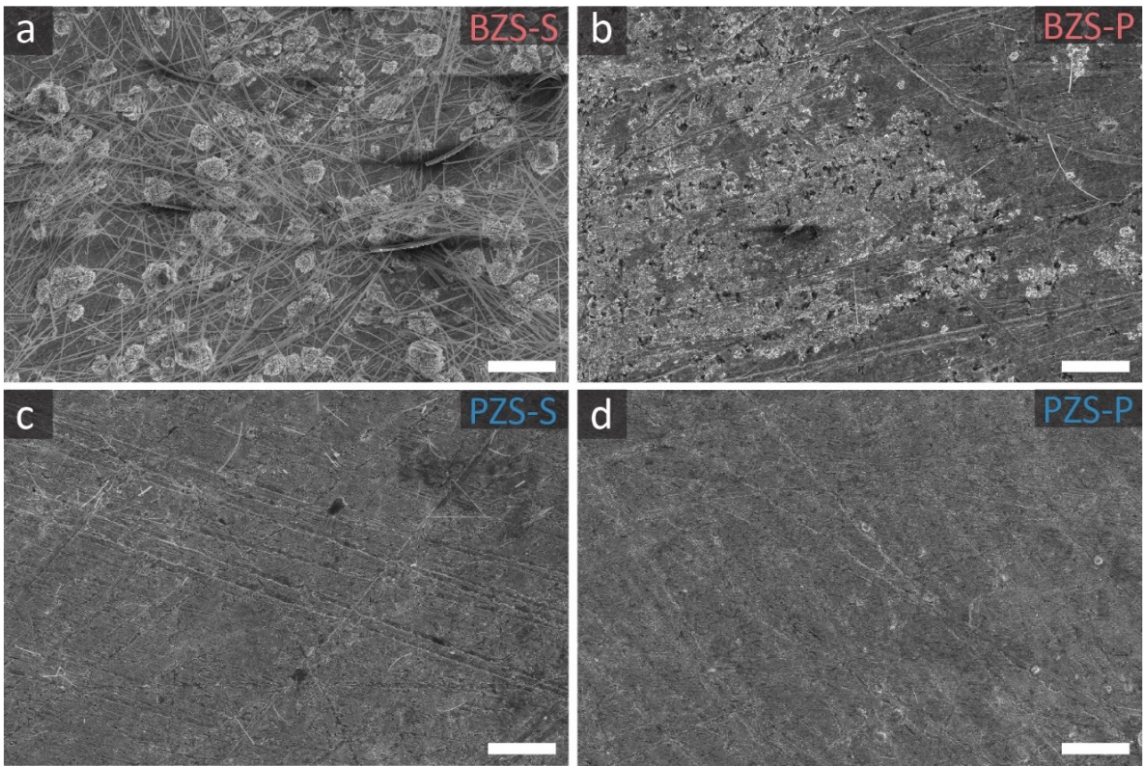

Supplementary Fig. 11 | Overall surface condition of cycled zinc electrodes. SEM images at a lower magnification showing stripped and plated electrodes in **a, b** Zn|BZS|Zn and **c, d** Zn|PZS|Zn symmetric cells. "-S" and "-P" denote the stripped and plated side in the last cycle, respectively. The scale bar measures 100 μm. BZS-S/P and HZS-S/P experienced 50 and 200 cycles at 1 mA cm^{-2}, 1mAh cm^{-2}, respectively.

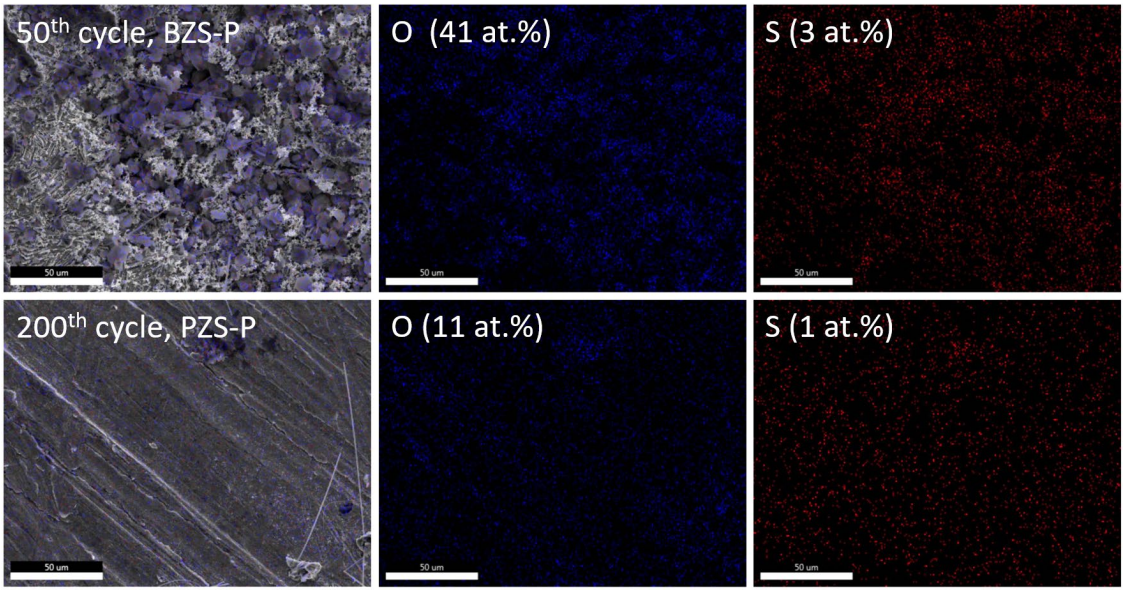

Supplementary Fig. 12 | SEM(-mapping) result. SEM and SEM-mapping of the plated side of Zn|BZS|Zn and Zn|PZS|Zn.

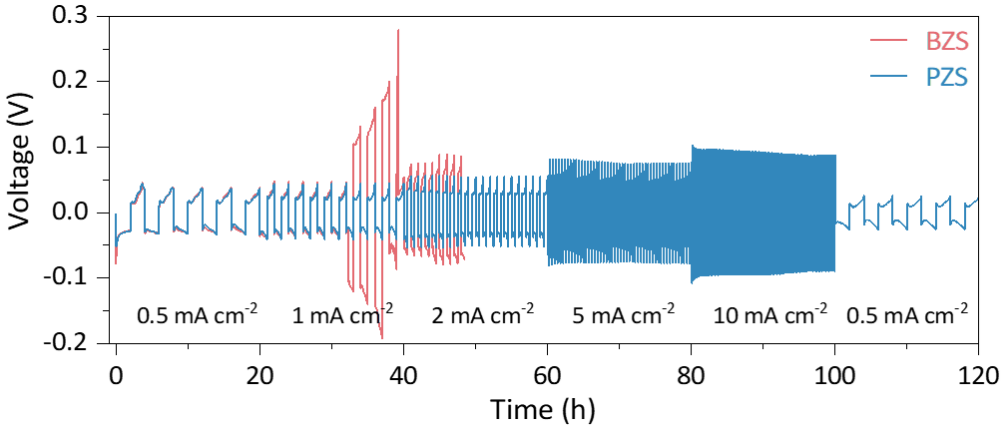

Supplementary Fig. 13 | Cycling performance. Cycling of Zn|BZS|Zn and Zn|PZS|Zn cells at a varying current density. The test was conducted at around 25 ºC with a cutoff voltage of ± 0.05 V.

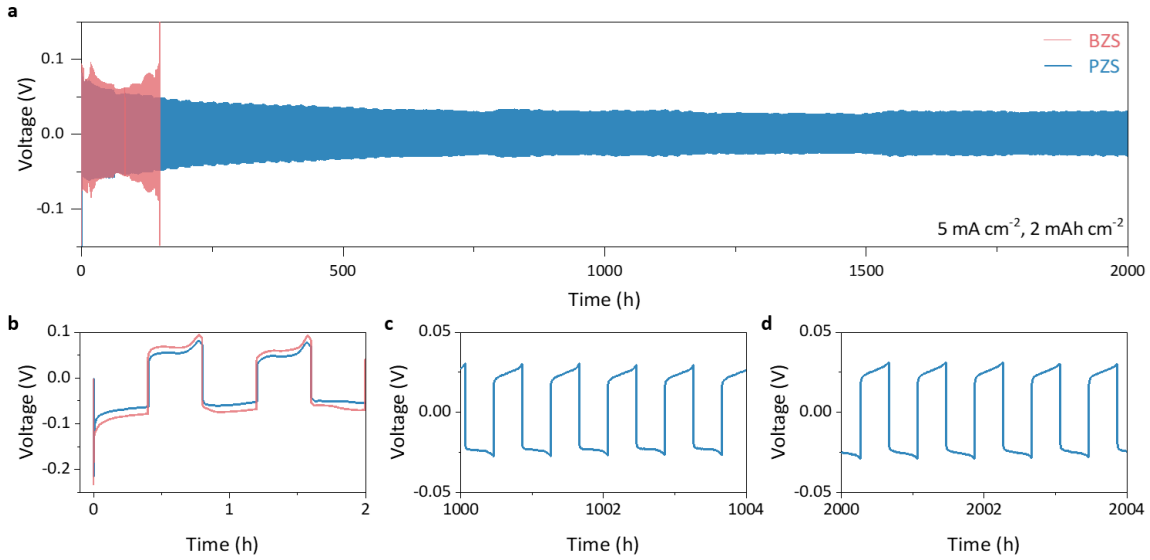

Supplementary Fig. 14 | Cycling performance at high current density. a Cycling of Zn|BZS|Zn and Zn|PZS|Zn cells at 5 mA cm^{-2}, 2 mAh cm^{-2} and **b-d** the corresponding enlarged curves at specific ranges. The test was conducted at around 25 °C with a cutoff voltage of ± 0.05 V.

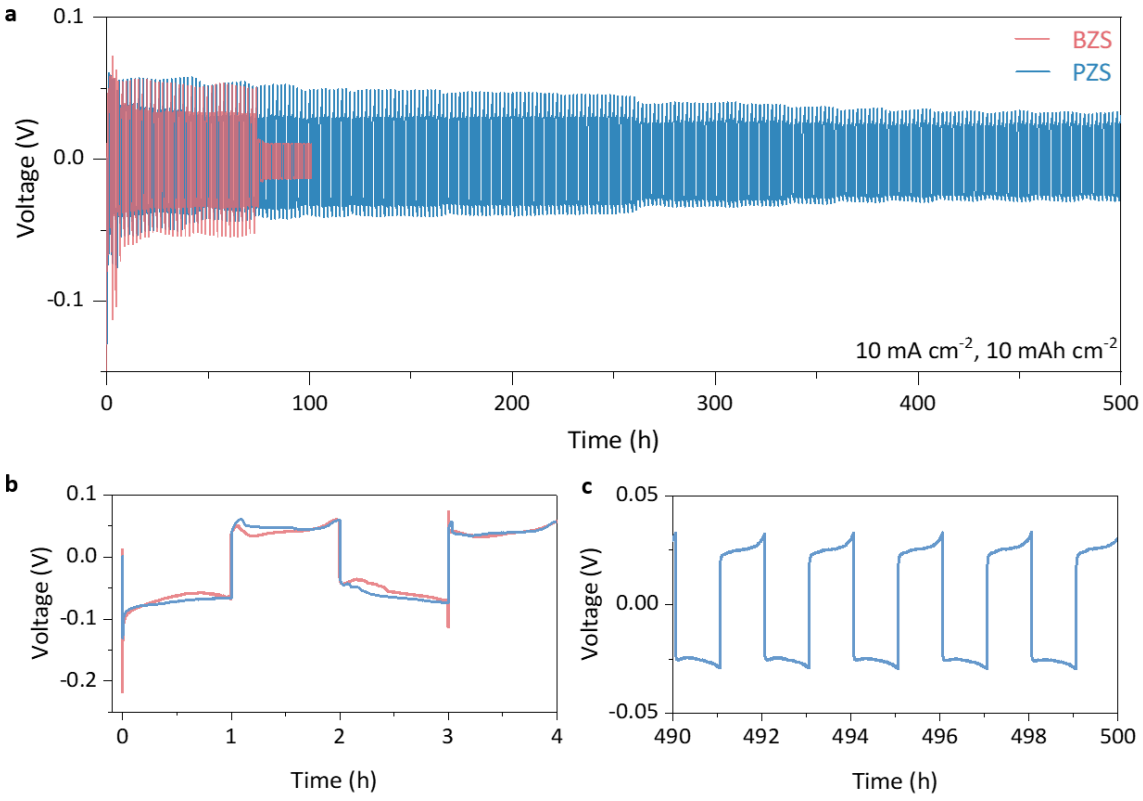

Supplementary Fig. 15 | Cycling performance in extreme conditions. a Cycling of Zn|BZS|Zn and Zn|PZS|Zn cells at 10 mA cm^{-2}, 10 mAh cm^{-2}, and **b, c** the corresponding enlarged spectra. The test was conducted at around 25 ºC with a cutoff voltage of ± 0.05 V.

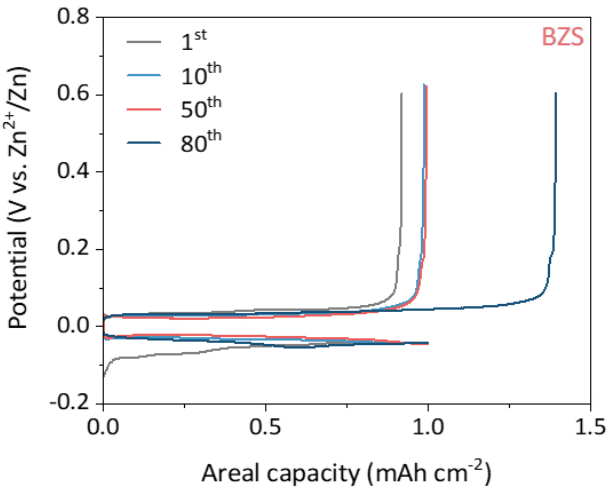

Supplementary Fig. 16 | Voltage profile of the Zn||Cu asymmetric cell. Selected charge-discharge curves of Zn|BZS|Cu asymmetric cells cycled at 1 mA cm^{-2}, 1 mAh cm^{-2}.

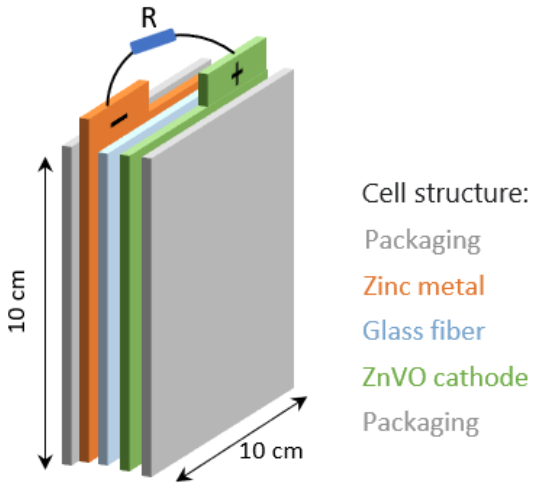

Supplementary Fig. 17 | Pouch cell configuration. The structure of the lab-scale Ah-level Zn|PZS|ZnVO pouch cell.

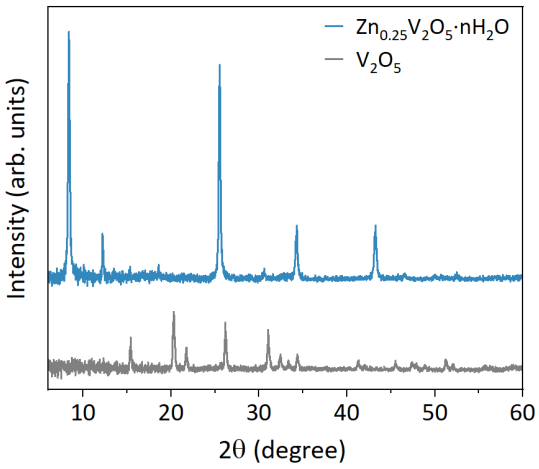

Supplementary Fig. 18 | Crystallinity properties of cathode materials. XRD patterns of the $Zn_{0.25}V_2O_5{\cdot}nH_2O$ and V_2O_5 powders.

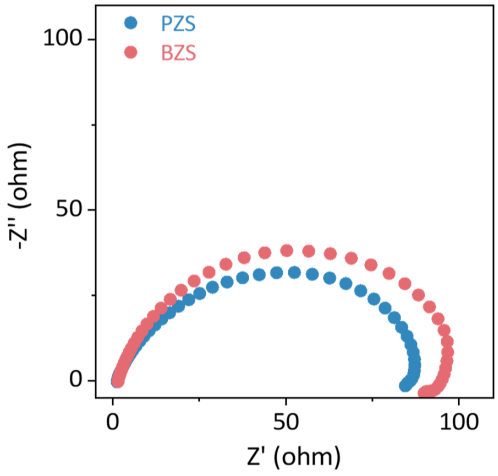

Supplementary Fig. 19 | EIS result of Zn||Zn symmetric cells. EIS spectra of cells based on BZS and PZS, respectively.

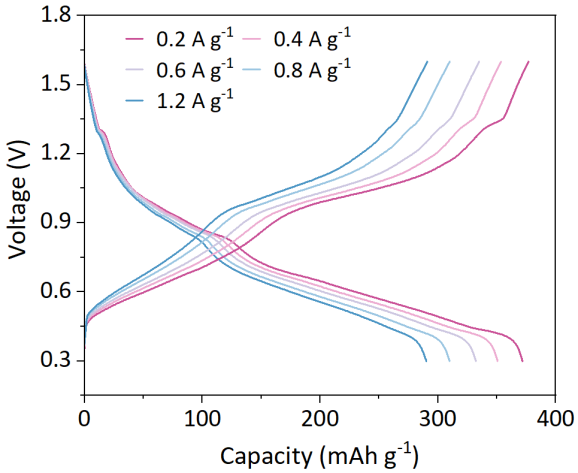

Supplementary Fig. 20 | Voltage profile of the full cell. GCD curves of Zn|PZS|$Zn_{0.25}V_2O_5{\cdot}nH_2O$ coin cell recorded at different charge densities. It is noted that the measurement was conducted at around 25 ^oC with a positive electrode mass loading of around 1.5 mg cm^{-2}.

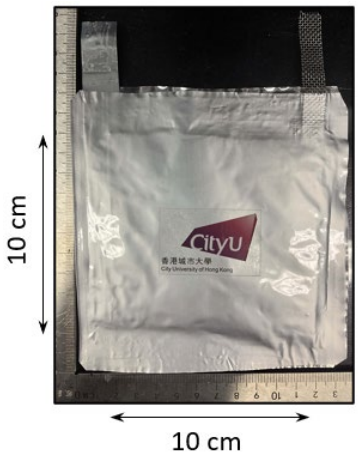

Supplementary Fig. 21 | Appearance of the pouch cell. Photograph of the Ah-level Zn|PZS|$Zn_{0.25}V_2O_5{\cdot}nH_2O$ pouch cell.

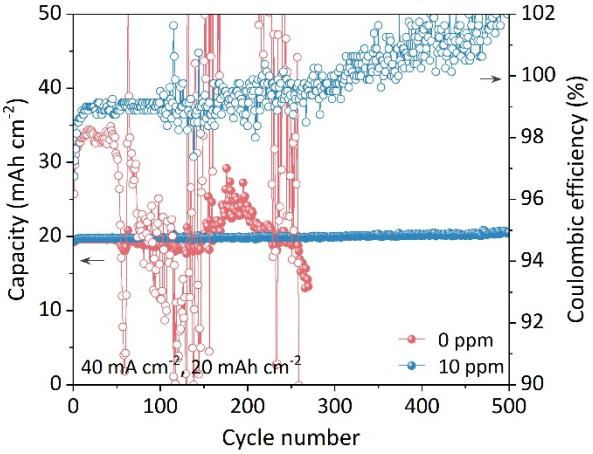

Supplementary Fig. 22 | Detailed evolution of coulombic efficiency demonstrated in Fig. 6b. Zn||CF flow batteries cycled at 40 mA cm^{-2}, 20 mAh cm^{-2}. It is noted that the measurement was conducted at around 25 °C with a flow rate of 50 mL/min, a charge cutoff capacity of 20 mAh cm^{-2}, and a discharge cutoff voltage of -0.5 V.

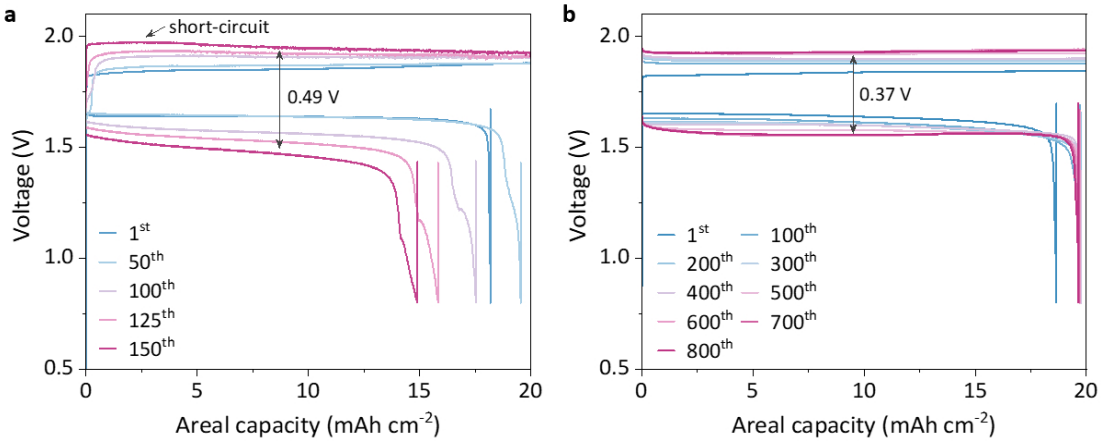

Supplementary Fig. 23 | Voltage profile of flow batteries. The GCD curves of Zn||Br_2 flow batteries **a** without and **b** with the addition of PPGA. It is noted that the measurement was conducted at around 25 °C with a flow rate of 50 mL/min, a charge cutoff capacity of 20 mAh cm^{-2}, and a discharge cutoff voltage of 0.8 V.